Exchange energy and stability diagram of few-electron coupled elongated quantum dots

L.-X. Zhang, D. V. Melnikov, and J.-P. Leburton

Beckman Institute for Advanced Science & Technology

and Department of Electrical and Computer Engineering,

University of Illinois at Urbana-Champaign, Urbana, Illinois 61801

(Dated: August 25, 2008)

Abstract

We study the properties of a few-electron system confined in coupled elongated quantum dots (QDs) using a model Gaussian potential and the numerical exact diagonalization technique. In the absence of magnetic fields, as the aspect ratio r between the QD extensions in the direction perpendicular and parallel to the coupling directions increases, the exchange energy exhibits a sharp variation at the specific value $r = 3.9$, before (after) which the exchange energy increases (declines). The sharp variation occurs because of a sudden change in the single-particle configuration of the triplet state. The stability region with one electron in each of the QDs is found to shrink, and finally vanishes as it becomes progressively easier to localize both electrons into the lower QD. For $r > 3.9$, the first singlet-triplet transition shifts to a small magnetic fields.

PACS numbers: 73.21.La, 73.21.-b

I. INTRODUCTION

Coupled quantum dots (QDs) based on two-dimensional electron gas (2DEG) formed with GaAs/AlGaAs heterostructures are promising candidates for quantum logic applications because of the ability to coherently manipulate the many-body spin states by using external electromagnetic fields.[1,2,3] Recently, a coherent controlled cycle of many-body state preparation, spin-interaction and projective read-out has been achieved in laterally coupled QDs.[4] In such an experiment, the electromagnetic control of the exchange energy J, which drives the Rabi oscillations between the lowest singlet and triplet states, is of utmost importance. It is well known that the hyperfine interaction between the electron and nuclear spins competes with the exchange energy to destroy the singlet-triplet coherence.[5] Therefore, in order to retain the spin-state coherence in coupled GaAs/AlGaAs QDs, it is important to optimize the exchange energy to exceed the hyperfine interaction significantly.

A wealth of theoretical work has been devoted to study the exchange energy in coupled QD systems.[6,7] The main focus of these studies is the tunability of the exchange energy by the electromagnetic fields and/or the parameters defining the interdot coupling strength, *e.g.*, interdot separation and barrier height. The optimization of the exchange coupling J—given a fixed interdot distance, which is predetermined by the lithography of the top gates—has been rarely discussed. In this work, we investigate such a possibility by considering QDs elongated perpendicularly to the coupling direction. In this configuration, one can expect the overlap between the electron wavefunctions in the two QDs to increase, which will enhance their interactions. Our work is encouraged by the recent proposal of using coupled elongated QDs to construct robust spin-qubits with all-electrical qubit manipulation capabilities.[8]

In this paper, we perform a detailed analysis of the two-electron system in coupled elongated QDs to show that the exchange coupling indeed becomes larger with increasing aspect ratio between the extensions of each QD perpendicular and parallel to the coupling direction ($r = R_y/R_x$). Our analysis based on the numerical exact diagonalization technique indicates that the cause of this enhancement is far from intuitive, while there is an optimum r value beyond which the exchange energy J decreases. Furthermore, for $r \geq 5$, we find that the stability region for one electron in each QD shrink to vanish. Finally, the magnetic field, which defines the boundary between different spin phases of the system ground state, decreases with increasing r.

II. MODEL AND METHOD

The Hamiltonian for the coupled QD system is given by

$$H = H_{orb} + H_Z, \tag{1}$$

$$H_{orb} = h(\mathbf{r_1}) + h(\mathbf{r_2}) + C(\mathbf{r_1}, \mathbf{r_2}), \tag{2}$$

$$h(\mathbf{r}) = \frac{1}{2m^*}(\mathbf{p} + \frac{e}{c}\mathbf{A})^2 + V(\mathbf{r}), \tag{3}$$

$$C(\mathbf{r_1}, \mathbf{r_2}) = e^2/\epsilon|\mathbf{r_1} - \mathbf{r_2}|, \tag{4}$$

$$H_Z = g\mu_B \sum_i \mathbf{B} \cdot \mathbf{S_i}. \tag{5}$$

Here, we use the material parameters of GaAs, electron effective mass $m^* = 0.067m_e$, dielectric constant $\epsilon = 12.9$, and g-factor $g = -0.44$. μ_B is the Bohr magneton, and $\mathbf{A} = \frac{1}{2}[-By, Bx, 0]$ is the vector potential for the constant magnetic field B oriented perpendicular to the QD plane (xy-plane). The Zeeman effect simply induces a lowering of the single-particle (SP) and triplet energies by 13 and 25 μeV/T, respectively.

We use the following model potential for the coupled QD system:[9]

$$\begin{aligned} V(\mathbf{r}) \;=\; & -V_L e^{-(x+d/2)^2/R_x^2 + y^2/R_y^2} \\ & -V_R e^{-(x-d/2)^2/R_x^2 + y^2/R_y^2}, \end{aligned} \tag{6}$$

where V_L and V_R are the depth of the left and right QDs (equivalent to the QD gate voltages in experimental structures[1]) which can be independently varied, d is the interdot separation, R_x and R_y are the radius of the each QD in the x and y direction, respectively. In this work, we fix $R_x = 30$ nm, and define QD *aspect ratio* $r = R_y/R_x$. Numerical exact diagonalization technique is used to solve for the single- and two-electron energies. Details of the method are published elsewhere.[9,10]

Upon completion of the diagonalization procedure, we extract the SP energies e_i and the two-particle energies $E_i^{S/T}$. Here, "S" ("T") denotes the singlet (triplet) state (In this paper, if not otherwise mentioned, "singlet" and "triplet" refer to the singlet and triplet states lowest in energy, respectively). The chemical potential of the N-th electron is given by the following equation:[1]

$$\mu(N) = E_0(N) - E_0(N-1), \tag{7}$$

where $E_0(N)$ [note $E_0(0) = 0$] refers to the ground state energy with N electrons in the system. The exchange energy is given by

$$J = E_0^T(2) - E_0^S(2). \tag{8}$$

For further analysis, the total energy of the two-electron system is partitioned into the expectation values of the SP energy K and Coulomb energy C

$$\begin{aligned} E^{S/T} &= \left\langle \Psi_0^{S/T} | H | \Psi_0^{S/T} \right\rangle \\ &= \left\langle \Psi_0^{S/T} | h(\mathbf{r_1}) + h(\mathbf{r_2}) | \Psi_0^{S/T} \right\rangle \\ &\quad + \left\langle \Psi_0^{S/T} | C(\mathbf{r_1}, \mathbf{r_2}) | \Psi_0^{S/T} \right\rangle \\ &= K^{S/T} + C^{S/T}, \end{aligned} \tag{9}$$

while the spectral function is defined as the projection coefficients of the lowest singlet and triplet states onto the SP product states[11]

$$\alpha_{k,l}^{S/T} = \left\langle \psi_k(\mathbf{r_1}) \psi_l(\mathbf{r_2}) | \Psi_0^{S/T}(\mathbf{r_1}, \mathbf{r_2}) \right\rangle. \tag{10}$$

The electron density is given by

$$\rho^{S/T}(\mathbf{r_1}) = \int |\Psi_0^{S/T}(\mathbf{r_1}, \mathbf{r_2})|^2 d\mathbf{r_2}. \tag{11}$$

Finally, the expectation value of the parity operator is given by

$$\begin{aligned} \left\langle \hat{P}^{S/T} \right\rangle &= \left\langle \Psi_0^{S/T}(x_1, y_1, x_2, y_2) \right. \\ &\qquad \left. \Psi_0^{S/T}(-x_1, -y_1, -x_2, -y_2) \right\rangle, \end{aligned} \tag{12}$$

and for the parity operator along the y-axis

$$\begin{aligned} \left\langle \hat{P}_y^{S/T} \right\rangle &= \left\langle \Psi_0^{S/T}(x_1, y_1, x_2, y_2) \right. \\ &\qquad \left. \Psi_0^{S/T}(x_1, -y_1, x_2, -y_2) \right\rangle. \end{aligned} \tag{13}$$

III. RESULTS

A. Aspect ratio dependence of the exchange energy

Figure 1 top panels show the potential contour plots $r = 1$ (left), $r = 4$ (middle), and $r = 8$ (right). As r increases, the potential becomes more elongated in the y-direction, while

the effective interdot distance (*i.e.*, the x-distance between the two minima of the potential) and the interdot barrier height remain constant at 40 nm and 1.98 meV, respectively.

In the lower panel of Fig. 1, we plot the three lowest singlet (red/gray, solid) and triplet (blue/dark gray, dashed) energy levels as a function of r. With increasing r, the SP energies decreases (not shown), resulting in the decrease of the two-particle energy levels. We note that the lowest energy of the singlet state $[E_0^S(2)]$ decreases smoothly with r, while the lowest energy of the triplet state $[E_0^T(2)]$ exhibits a cusp at $r = 3.9$ because of the crossing of the lowest two triplet state energy levels. This cusp results in a sharp variation in the exchange energy dependence on r, which is shown in the inset of the lower panel of Fig. 1. In the same inset, we show the variation of the tunnel coupling $2t = e_1 - e_0$. For $r \leq 4.3$, the SP ground and first excited states have s and p_x characters, respectively, and $2t$ barely increases from 1.8105 to 1.8114 meV with increasing r, because the energy contributions from the y-direction to e_0 and e_1 cancel out. For $r > 4.3$, the SP first excited state bears a p_y character, which causes $2t$ to decrease monotonically with r.

In order to investigate in detail the cusp in the lowest triplet state energy, or, the crossing between the two lowest triple levels in the lower panel of Fig. 1, we plot in Fig. 2 the spectral function of the two-electron wavefunction. It is seen that at $r = 3.9$ the triplet mainly consists of the $[1, 2]$ and $[2, 1]$ SP state pair, while at $r = 4$ it mainly consists of the $[1, 3]$ and $[3, 1]$ SP state pair. Here, 1, 2 and 3 denote the SP states in ascending energy, which have s, p_x and p_y characters, respectively, as shown in the Fig. 2 inset. Since the energy ordering of these SP states does not change as r changes from 3.9 to 4 (not shown here), the cusp in the lowest triplet state is due to a sudden transition of the triplet wavefunction from occupying an sp_x pair to an sp_y pair.

In Fig. 3, we plot separately the (a) SP $< K >$ and (b) Coulomb $< C >$ contributions to the singlet and triplet state energies as a function of the QD aspect ratio r. As r increases, the general trend for all these energy terms is to decrease, leading to decreasing singlet and triplet energies shown in Fig. 1. For the singlet state, both $< K >$ and $< C >$ terms decrease smoothly with r. For the triplet state, however, a discontinuity is seen from $r = 3.9$ to 4: $< K >$ ($< C >$) suddenly increases (decreases) by 0.128 (0.607) meV. It now becomes clear that the transition of the SP configuration shown in Fig. 2 from the sp_x pair to the sp_y pair is favored by the lowering of the Coulomb interaction despite the increase in the SP energy. The insets in Fig. 3(a) and (b) show that the difference in the Coulomb energy

between singlet and triplet states ($\Delta C = \langle C^T \rangle - \langle C^S \rangle < 0$) is always overcome by the SP energy contribution ($\Delta K = \langle K^T \rangle - \langle K^S \rangle > 0$), leading to a positive exchange interaction ($J = \Delta K + \Delta C$, see Fig. 1).[12] The comparison between ΔK and the tunnel coupling $< 2t >$ in the inset of Fig. 3(a) shows that the SP energy contribution to the singlet and triplet states is strongly influenced by the Coulomb interaction and is quite different from the noninteracting picture.

As a consequence of the sudden change in the SP occupation, the y-symmetry P_y of the two-electron wavefunction of the lowest triplet state changes abruptly from 1 to -1, which is validated by direct calculation of P_y. We point out that the crossing between the lowest two triplet states by increasing r is allowed because they possess opposite y-symmetry, which exemplifies the general von Neumann-Wigner theorem relating the molecular energy levels to the two-electron wavefunction symmetry.[13]

The contour plots in Fig. 4 clearly show that from $r = 3.9$ (first row) to $r = 4$ (second row) the electron density in the lowest singlet state barely changes, while the density in the lowest triplet state changes abruptly from two peaks localized in the left and right QDs (the separation of two peaks in the x-direction is ~ 40 nm) to four peaks separated along both x and y directions (separation between peaks in the x and y directions are 20 and 40 nm, respectively), again due to the sudden change in the SP configuration. The third row in Fig. 3 shows that at $r = 8$, both the singlet and triplet densities exhibit four peaks separated in both the x and y directions. Our analysis shows that from $r = 4$ to $r = 8$, the left and right peaks in the singlet state density gradually separate into four peaks, and the separation between the top two and bottom two peaks in the triplet state density smoothly increases. Such electron localization effects at large r are discussed for other many-electron QD systems with weak confinement, see, *e.g.* Ref. 14 and references therein.

B. Stability diagrams

In Fig. 5, upper panels, we plot the stability diagrams[1] of the coupled QDs for $r = 1$ (left), $r = 3$ (middle), and $r = 5$ (right) for $R_x = 30$ nm, $d = 50$ nm and $B = 0$ T. The solid curves indicated by arrows shows the computed contours, where chemical potentials of the first electron (red), the second electron in the singlet state (green), and second electron in the triplet state (blue) are equal to the reference value [$\mu(1) = \mu^S(2) = \mu^T(2) = -21$

meV]. According to the general shape of the stability diagram for coupled QDs,[1] we use dotted straight lines on the diagrams to separate different charge states indicated by discrete electron numbers on the left and right QDs, *e.g.*, $(0,1)$ means zero electrons on the left QD and one electron on the right QD. Specifically, the boundaries between the $(1,1)$ and $(0,2)$ [or $(2,0)$] states are taken extending from the point on the $\mu^S(2)$ curve at which the curvature is the largest for $V_L \neq V_R$, *e.g.*, point C on the upper left panel and parallel to the main diagonal. In the absence of magnetic field ($B = 0$), the $\mu^S(2)$ curve is the boundary between one and two electrons in the system (in the linear transport regime wherein the source and drain chemical potentials are nearly the same).[12] Based on this fact, we extrapolate from the first off-diagonal triple point (*e.g.*, point C on the upper left panel) to get the boundary between two- and three-electron states [green dotted curve indicated by $\mu(3)$]. Here, we assume that the triple point separation between charge states $(1,0)$ and $(2,1)$ (or between the $(0,1)$ and $(1,2)$) is the same as the separation between the $(0,0)$ and $(1,1)$ states.[15]

In Fig. 5, we notice that, on the one hand, as r increases, the crossing points of the $\mu(1)$, $\mu^S(2)$ and $\mu^T(2)$ curves with the main diagonal shift to smaller $V_L = V_R$ values because the SP energies decreases as r increases, and as such a less negative V_L and V_R value is required to charge the coupled QDs. On the other hand, the double-triple point (DTP) separation, *i.e.*, the separation between the crossing points of $\mu(1)$ and $\mu(2)$ curves with $V_L = V_R$, decreases with r. For the singlet (triplet) state, the DTP separation measured in $\Delta V_L = \Delta V_R$ is 5.181 (5.269), 4.128 (4.725) and 3.473 (3.907) for $r = 1$, 3 and 5, respectively. This decreasing trend of the DTP separation suggests that the coupling strength between the two QDs decreases with increasing r (see Ref. 1). However, from our direct calculations shown in the inset of Fig. 1, lower panel, the tunnel coupling decreases only for $r > 4.3$, while the exchange energy is largest for $r = 3.9$. The discrepancies regarding the coupling strength between the DTP separation and direct calculations of the tunnel and exchange couplings can be understood by observing the following: the DTP separation is given by $2t + C$, where $2t$ and C denote tunnel coupling and interdot Coulomb interaction. As r increases $2t$ decreases for $r > 4.3$, while $< C >$ monotonically decreases for both singlet and triplet (see Fig. 3). As a result, the DTP separation decreases. The exchange coupling, however, is determined by the energy *difference* between the singlet and triplet states. As shown in Fig. 3, such energy difference, when splitted into the SP contribution $< \Delta K >$ and the Coulomb contribution $< \Delta C >$, has a complicated dependence on r. In contrast,

if the interdot separation were increased to decouple the two QDs, then all quantities $2t$, C, $<\Delta K>$, and $<\Delta C>$ would decrease, leading to both decreasing DTP separation and exchange energy.[7,11]

One important feature shown in Fig. 5 is that as r increases, the distance between the triple points on the main diagonal and the first off diagonal (*e.g.*, points B and C in the upper left panel of Fig. 5) becomes smaller, and at large r these triple points coincide. Consequently, the $(1,1)$ stability region shrinks and finally disappears. This is because at large aspect ratios, even a small amount of interdot detuning can localized both electrons into the lower QD, resulting in an unstable $(1,1)$ charge state. The boundary $\mu^T(2)$ at $r = 5$ suggests that the $(1,1)$ charge state is also unstable for the triplet state, although the $\mu^S(2)$ and $\mu^T(2)$ curves evolve in different fashion as r increases.

After locating the different charge stable regions on the stability diagram, we now investigate the interdot detuning effect by departing from the center of the $(1,1)$ region along the direction perpendicular to the main diagonal, *i.e.*, $V_L + V_R = constant$. Such detuning effects are important as two electrons transfer to a single QD, which is a key step in spin coherent manipulation and spin-to-charge conversion in two-electron double QD experiments for quantum logic gate applications.[2,4]

The solid curves in Fig. 5, lower panels, show the exchange energy J as a function of interdot detuning $\epsilon = V_L - V_R$ along the $V_L + V_R = constant$ line [$\epsilon = 0$ is chosen at the $(1,1)$ region center]. In the case of coupled circular QDs ($r = 1$), both singlet and triplet states localize progressively into the lower QD with increasing ϵ, leading to a monotonic increase of J. Such a dependence is similar to recent experimental[4] and theoretical[16] results. For $r = 3$, a sharp cusp in J occurs at $\epsilon \sim 4$ meV before which J monotonically increases with ϵ. This cusp is induced by a sudden SP configuration change in the lowest triplet state, which is similar to the effects seen in Fig. 1 and analyzed in Fig. 2, albeit here the perturbation in the Hamiltonian is introduced by interdot detuning instead of deformation effects. More detailed analysis of the two-particle energies and electron density for the $r = 1$ and $r = 3$ cases can be found in Ref. 17. For $r = 5$, we observe that the exchange energy decreases monotonically with ϵ, because the Coulomb energy difference between the singlet and triplet states becomes smaller as the two electrons in both the singlet and triplet states localize at the opposite ends of the lower single QD to minimize their Coulomb interaction.

In the lower panels of Fig. 5, we also plot the ϵ dependence of Δ^{ST} (dashed curves), the

difference between the $\mu^S(2)$ and $\mu^T(2)$ curves projected along the main diagonal. Δ^{ST} is relevant in this context because in coupled QD experiments the chemical potential contour lines are mapped out by single-electron charging measurements, which provides useful information on the electronic structure of the QD.[1,2,18] Here, we notice that although the general detuning dependence is similar between J and Δ^{ST}, a linear factor is not sufficient to scale values of J to overlap with those of Δ^{ST} because the two quantities are extracted under different bias conditions. It should be pointed out that transport experiments measure the quantity Δ^{ST}, which differs quantitatively from the exchange energy J.

In Fig. 6, we plot the charge stability diagram of the coupled QDs for $r = 1$ (left), $r = 3$ (middle), and $r = 5$ (right) for $R_x = 30$ nm, $d = 60$ nm and $B = 0$ T. Compared to the data in Fig. 5, which correspond to strongly coupled QDs, the data in Fig. 6 depict the situation in decoupled QDs.[7] In this case, as r increases, (1) the crossing points of the $\mu(1)$, $\mu^S(2)$ and $\mu^T(2)$ curves with the main diagonal shift to smaller $V_L = V_R$ values; (2) the DTP separation decreases [The DTP separation is 2.847 (2.860), 2.618 (2.641), 2.514 (2.545), for $r = 1$, $r = 3$, and $r = 5$, respectively]; and (3) the $(1, 1)$ region becomes smaller. These behaviors are similar to those for $d = 50$ nm. However, the $(1, 1)$ region does not vanish at $d = 60$ nm and $r = 5$ because as the QDs are more decoupled, both the interdot distance and interdot barrier height become larger, which require a larger interdot detuning to "push" both electrons into the lower QD. At a fixed r, the DTP separation (curvature at the triplet points) is smaller (larger) for $d = 60$ nm than for $d = 50$ nm, indicating that both tunnel coupling and Coulomb interaction are smaller for more decoupled QDs.[7]

C. Spin phase diagram

In this subsection, we discuss the variation of the exchange energy J as a function of both r and B. By identifying the regions where J assumes different signs, we construct the spin phase diagram in which the two-electron ground state spin state (either $S = 0$ or $S = 1$) is shown as a function of r and B.[19,20]

In Fig. 7, we plot the exchange energy J as a function of the QD aspect ratio r and the magnetic field B perpendicular to the xy-plane. At fixed r, as B increases, J decreases from its value at $B = 0$ T to become negative and saturate at very large magnetic field, as previously reported.[6] We note that at intermediate r ($r \sim 4$), J changes much faster with B

than at small or large r. This B-field effect at intermediate r values is associated with the 2D confinement of the QDs, *i.e.*, near $r = 4$ the SP level separations in the x- and y-directions are comparable (cf. Fig. 1, lower inset, $2t$ curve). We also note that, with increasing r, the relative change of J is small for $B \sim 1$ T, while it is much larger for $B \sim 0$ T or $B \sim 2$ T. The kink in J at $B = 0$ T (cf. Fig. 1, lower inset, J curve), due to the crossing of two lowest triplet levels, does not exist for $B \neq 0$ T because a nonzero magnetic field couples the SP states with different Cartesian symmetries, thereby removing the condition for the crossing of the lowest two triplet states. In the investigated ranges of r and B, J assumes a maximum (minimum) value of 0.773 (-0.372) meV at $r \approx 3.9$, $B \approx 0$ T ($r \approx 4.4$, $B \approx 1.6$ T).

The projected contour plots in Fig. 7 shows that the first singlet-triplet transition (at which J first crosses zero as B increases from zero at fixed r) occurs at a smaller B value as r increases, which is shown by the thick white dashed curve on the contour plot in Fig. 7. Such a dependence can be understood by observing that, in the absence of the B field, as r increases the SP energy spacing decreases, and, for a larger r, a smaller magnetic field is needed to further decrease the SP spacing and bring the triplet state to the ground state with the aid of the Coulomb energy difference between the singlet and triplet states. At higher magnetic field and larger r, we observe another contour line for $J = 0$ (thick solid white curve at the lower left corner). The reappearance of the singlet state as the ground state is reminiscent of the singlet-triplet oscillation found for a two-electron single QD and also reported elsewhere for two-electron QDs with strong confinement.[19,20,21] In the foregoing discussion, we had not included the Zeeman energy for the triplet state, which would lower the triplet energy such that the boundary for the first singlet-triplet transition (thick white dashed curve) would shift to lower values of r and B, while the second singlet-triplet transition (thick white solid curve) would move to higher values of r and B.

IV. CONCLUSIONS

We have shown that the exchange energy between two electrons in coupled elongated quantum dots is enhanced by increasing the aspect ratio of the dots in the perpendicular direction to the coupling direction. However, there is an optimum aspect ratio beyond which the electron density in each dot starts to localize, and the exchange energy decreases.

With increasing aspect ratio, the $(1,1)$ region becomes unstable with respect to interdot detuning, which is undesirable for two spin-qubit operations. We have also shown that the exchange energy in symmetrically biased coupled quantum dots is tunable between maximum (positive) and minimum (negative) values by varying the magnetic field and the QD aspect ratio.

Acknowledgments

This work is supported by the DARPA QUIST program and NSF through the Material Computational Center at the University of Illinois. LXZ thanks the Beckman Institute, Computer Science and Engineering program, and the Research Council at the University of Illinois.

---

[1] W. G. van der Wiel, S. D. Franceschi, J. M. Elzerman, T. Fujisawa, S. Tarucha, and L. P. Kouwenhouven, Rev. Mod. Phys. **75**, 1 (2003).

[2] R. Hanson, L. P. Kouwenhoven, J. R. Petta, S. Tarucha, and L. M. K. Vandersypen, Rev. Mod. Phys. **79**, 1217 (2007).

[3] D. Loss and D. P. DiVincenzo, Phys. Rev. A **57**, 120 (1998).

[4] J. R. Petta, A. C. Johnson, J. M. Taylor, E. A. Laird, A. Yacoby, M. D. Lukin, C. M. Marcus, M. P. Hanson, A. C. Gossard, Science **309**, 2180 (2005).

[5] E. A. Laird, J. R. Petta, A. C. Johnson, C. M. Marcus, A. Yacoby, M. P. Hanson, and A. C. Gossard, Phys. Rev. Lett. **97**, 056801 (2006).

[6] G. Burkard, D. Loss, and D. P. DiVincenzo, Phys. Rev. B **59**, 2070 (1999); W. Dybalski and P. Hawrylak, Phys. Rev. B **72**, 205432 (2005); X. Hu and S. Das Sarma, Phys. Rev. A **61**, 062301 (2000); B. Szafran, F. M. Peeters, and S. Bednarek, Phys. Rev. B **70**, 205318 (2004); D. Bellucci, M. Rontani, F. Troiani, G. Goldoni, and E. Molinari, Phys. Rev. B **69**, 201308(R) (2004); J. Pedersen, C. Flindt, N. A. Mortensen, and A.-P. Jauho, Phys. Rev. B **76** , 125323 (2007); A. Harju, S. Siljamäki, and R. M. Nieminen, Phys. Rev. B **65** , 075309 (2002).

[7] L.-X. Zhang, D. V. Melnikov, and J.-P. Leburton, Phys. Rev. B **74**, 205306 (2006).

[8] J. Kyriakydis and G. Burkard, Phys. Rev. B **75**, 115324 (2007).

[9] L.-X. Zhang, D. V. Melnikov and J.-P. Leburton, IEEE Trans. Nanotechnol. **6**, 250 (2007).

[10] D. V. Melnikov and J.-P. Leburton, Phys. Rev. B **73**, 085320 (2006).

[11] D. V. Melnikov and J.-P. Leburton, Phys. Rev. B **73**, 155301 (2006).

[12] For two electrons under zero magnetic field, the singlet state is always the ground state, see, *e.g.*, N. W. Ashcroft and N. D. Mermin, *Solid State Physics* (Brooks/Cole, Thomson Learning, Cornell, 1976), for which reason the triplet state bears less interest in the absence of magnetic field. Nevertheless, we discuss the triplet as a comparison to the singlet state.

[13] J. von Neumann and E. Wigner, Z. Phys. **30**, 467 (1929); L. D. Landau and E. Lifshitz, *Quantum Mechanics: Non-Relativistic Theory* (Pergamon Press, Oxford, 1977).

[14] S. Bednarek, T. Chwiej, J. Adamowski, and B. Szafran, Phys. Rev. B **67**, 205316 (2003).

[15] We emphasize that the boundary between two- and three-electron states are *not* computed. In other words, the $\mu(3)$ curves on the diagrams are guides to the eyes to delimit the charge states for two electrons in the coupled QDs.

[16] M. Stopa, C.M. Marcus, Nano Lett. **8** 1778, (2008).

[17] L.-X. Zhang, D. V. Melnikov and J.-P. Leburton, Phys. Rev. B **78**, 085310 (2008). In this reference, the detuning is measured by fixing $V_R = constant$, while in the text, it is measured perpendicular to the main diagonal of the stability diagram, *i.e.,* $V_L + V_R = constant$.

[18] A. C. Johnson, J. R. Petta, C. M. Marcus, M. P. Hanson, and A. C. Gossard, Phys. Rev. B **72**, 165308 (2005).

[19] A. Harju, S. Siljamäki, and R. M. Nieminen, Phys. Rev. Lett. **88**, 226804 (2002).

[20] M. Helle, A. Harju and R. M. Nieminen, Phys. Rev. B **72**, 205329 (2005).

[21] M. Wagner, U. Merkt and A. V. Chaplik, Phys. Rev. B **45**, 1951 (1992).

Figures

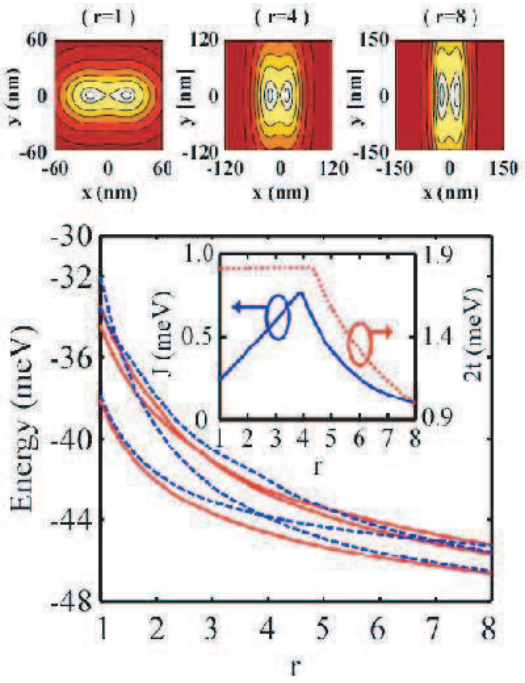

FIG. 1: (Color online) Top panels: potential contour plots of coupled QD with $r = 1$ (left), $r = 4$ (middle), and $r = 8$ (right). Redder (darker gray) regions correspond to higher potential. Bottom panel: three lowest singlet (red/gray, solid lines) and triplet (blue/dark gray, dashed lines) energy levels as a function of QD aspect ratio r. The inset shows r dependence of the exchange energy J (blue/dark gray, solid) and tunnel coupling $2t$ (red/gray, dotted). For all panels, $V_L = V_R = 25$ meV, $d = 50$ nm, $B = 0$ T.

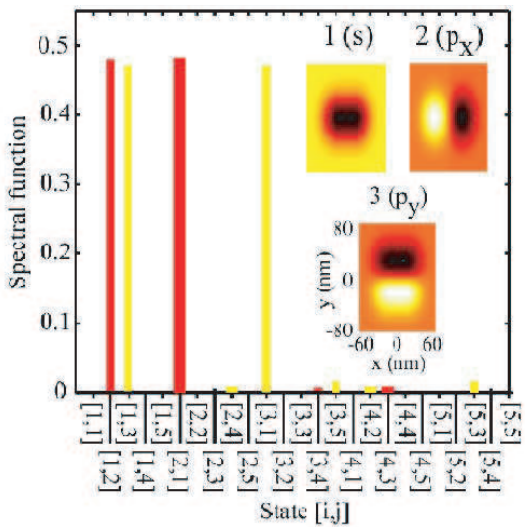

FIG. 2: (Color online) Spectral decomposition of the two-electron wavefunction onto different single-particle pairs. The red (dark) columns are for $r = 3.9$, while the yellow (bright) columns are for $r = 4$. The inset shows the contour plots of lowest three single-particle states in ascending order (indicated by number) of energy for both $r = 3.9$ and $r = 4$. The state symmetry is shown in parenthesis.

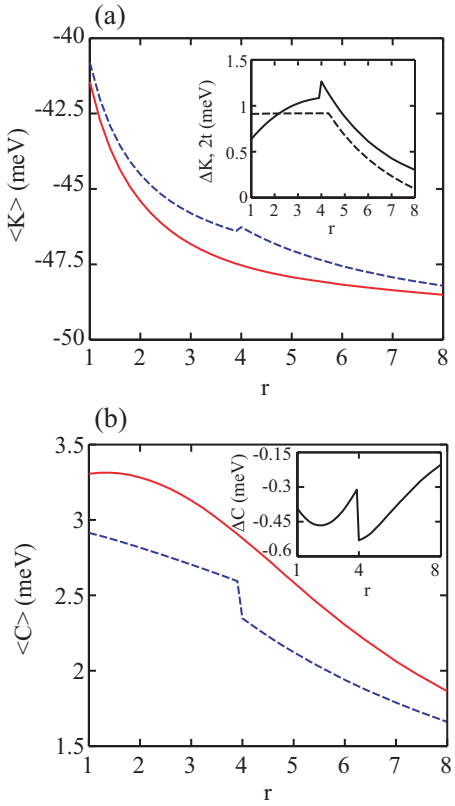

FIG. 3: (Color online) (a) Single-particle energy contribution $\langle K \rangle$ as a function of QD aspect ratio r. The red/gray, solid (blue/dark gray, dashed) line is for the singlet (triplet) state. Inset: the solid line shows the difference $\Delta K = \langle K^T \rangle - \langle K^S \rangle$. The dashed line shows $2t$ as a comparison. (b) Coulomb energy contribution $\langle C \rangle$ as a function of QD aspect ratio r. The red/gray, solid (blue/dark gray, dashed) line is for the singlet (triplet) state. Inset: the solid line shows the difference $\Delta C = \langle C^T \rangle - \langle C^S \rangle$.

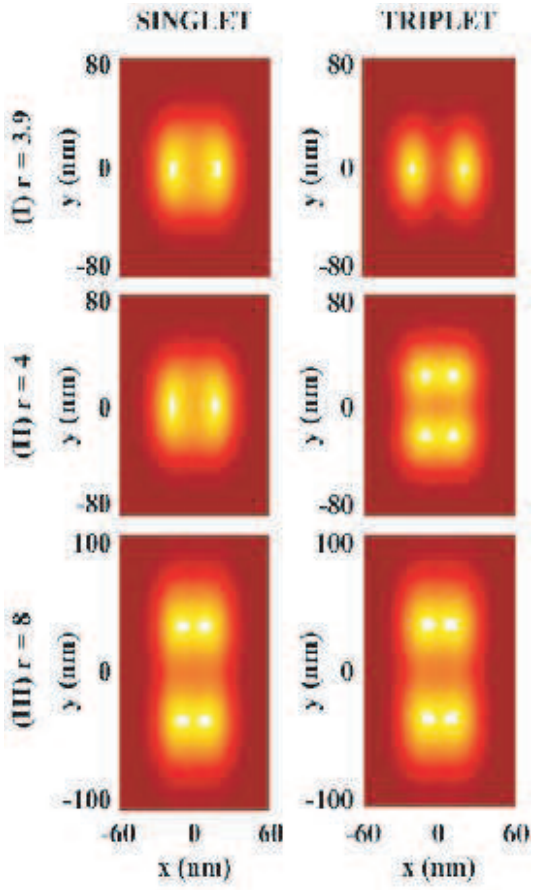

FIG. 4: (Color online) Contour plots of the electron density for both singlet (left column) and triplet (right column). Rows I, II and III are for $r = 3.9$, $r = 4$ and $r = 8$, respectively. In the plots, redder (darker gray) regions correspond to lower electron density.

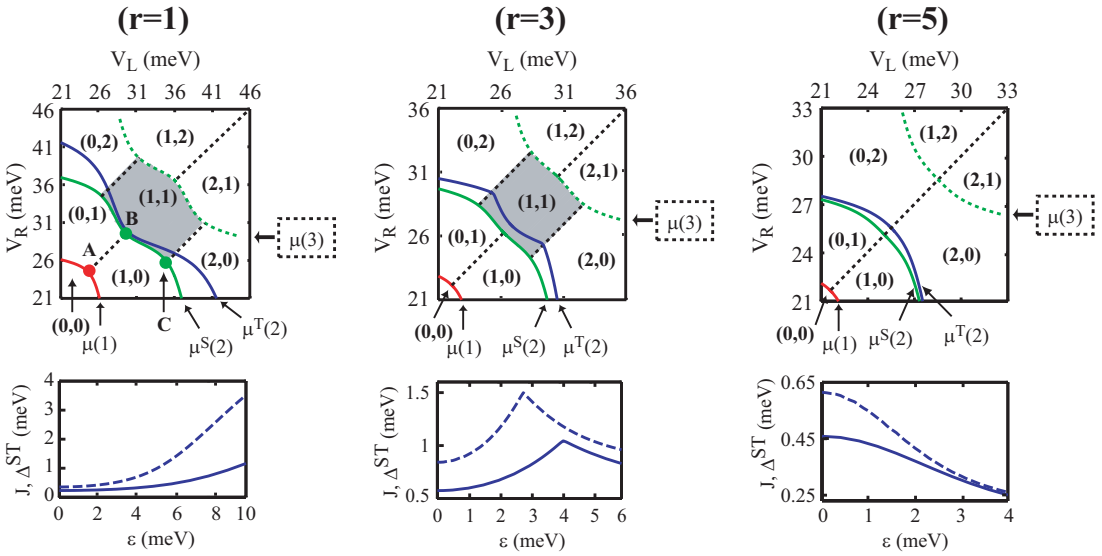

FIG. 5: (Color online) Top panels: stability diagrams for $r = 1$ (left), $r = 3$ (middle) and $r = 5$ (right). In each diagram, the red, green and blue curves (solid) are computed contour lines at which the chemical potential $\mu(1)$, $\mu^S(2)$ and $\mu^T(2)$ equal to the reference value $\mu_{ref} = -21$ meV, respectively. Curves for different chemical potentials are also indicated by arrows. The dotted straight lines are a guide for eyes separating different stable charge states. Note that the exact locations of the $\mu(3)$ curve (green dotted curve) and $(1, 2)$, $(2, 1)$ regions are not computed. In the left two top panels, the $(1, 1)$ region is indicated by the shaded area. In the left most upper panel, we also indicate the double-triple points A and B. Point C is where the $\mu^S(2)$ curve has the largest curvature for $V_L \neq V_R$. For corresponding QD aspect ratios, the bottom panels show J (solid curves) as a function of interdot detuning $\epsilon = V_L - V_R$ from the center of the $(1, 1)$ region. The dashed curves on the bottom panels show the separation (Δ^{ST}) between the contour lines of $\mu^S(2)$ and $\mu^T(2)$ projected along the main diagonal of as a function of interdot detuning $\epsilon = V_L - V_R$. All data are obtained at $R_x = 30$ nm, $d = 50$ nm and $B = 0$ T.

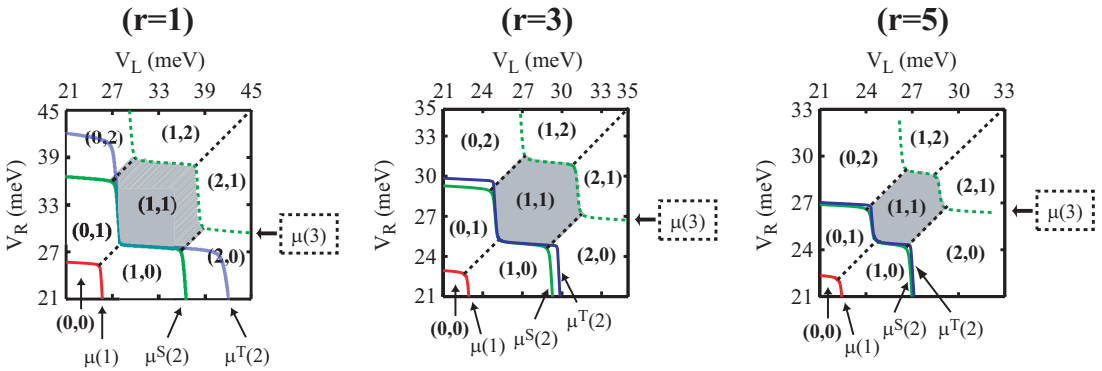

FIG. 6: (Color online) Stability diagrams for $r = 1$ (left), $r = 3$ (middle) and $r = 5$ (right). In each diagram, the red, green and blue curves (solid) are computed contour lines at which the chemical potential $\mu(1)$, $\mu^S(2)$ and $\mu^T(2)$ equal to the reference value $\mu_{ref} = -19$ meV, respectively. Curves for different chemical potentials are also indicated by arrows. The dotted straight lines are a guide for eyes separating different stable charge states. Note that the exact locations of the $\mu(3)$ curve (green dotted curve) and $(1, 2)$, $(2, 1)$ regions are not computed. In each panel, the $(1, 1)$ region is indicated by the shaded area. All data are obtained at $R_x = 30$ nm, $d = 60$ nm, and $B = 0$ T.

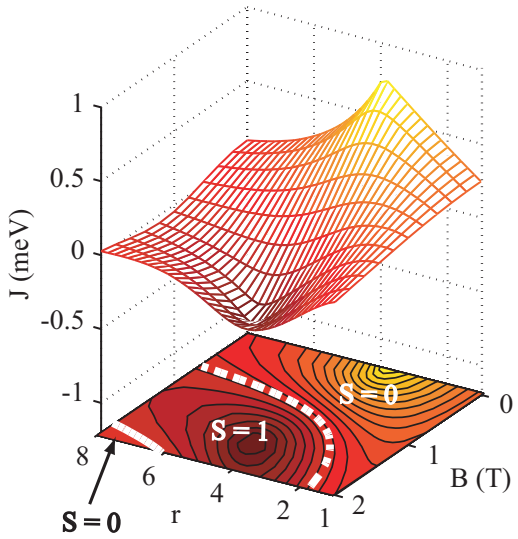

FIG. 7: (Color online) Mesh (contour) plot of the exchange energy J as a function of QD aspect ratio r and the magnetic field B. The thick white curves (solid and dashed) on the contour plot correspond to $J = 0$. Total spin of the two-electron ground state is given in different regions. Redder (darker gray) regions correspond to lower J value.